Intra-Operative Optical Coherence Imaging of *In-Vivo* Chronic Otitis Media Followed by Post-Operative Audiogram Assessments

Hayoung Kim, Jaeyul Lee, Ruchire Eranga Wijesinghe, Jeong Hun Jang, Mansik Jeon, *Member, IEEE*, and Jeehyun Kim, *Member, IEEE*

***Abstract*—The successful surgery of chronic otitis media (COM) is challenging; this depends on the surgeon's knowledge of the optical visibility of surgical microscopes. Herein, we reported the utilization of intra-surgical optical coherence tomography (OCT) system to effectively guide the surgery of COM based on augmented reality with cross-sectional images. The intra-surgical spectral-domain OCT system with a center wavelength of 846 nm was capable of obtaining non-invasive, high-resolution, and high-speed visualizations with an axial resolution of 8 μm, lateral resolution of 30 μm, and an extended working distance of 280 mm. Three patients with COM were involved in this research. The lesion conditions of the temporal bone were observed with computed tomography pre-operatively. Furthermore, pure-tone audiogram examinations were performed to evaluate pre and post-surgical conditions. The results revealed that the averaged air-bone gap of 500 Hz, 1 kHz, 2 kHz, and 4 kHz in all cases improved to 61%. Thus, the research proves that the experimental procedure can be beneficial and clinically applicable with the developed intra-surgical OCT system for future otolaryngological assessments.**

***Index Terms*—Optical coherence tomography, chronic otitis media, surgical guidance, audiogram diagnostics, transplantation.**

I. Introduction

THE middle ear, which is anatomically located between the outer and inner ear consists of the tympanic membrane (TM), ossicles, and ear canal [1]–[3]. Chronic otitis media (COM) is a chronic inflammation of the middle ear cavity including mucosa and TM. Recurrent inflammation causes the TM perforations and otorrhea, such as dirt and pus are repeatedly secreted [4], [5]. Several important factors influence the chronicization of otitis media (OM) [6]; the most common and important of which is the infection by bacterial micro-organisms. Bacteria entering the middle ear cause irritation to the mucosa of the middle ear, which causes the TM and the ossicles to become increasingly injured [7]–[9]. As the disease progresses through the perforation of the TM, the hearing level is aggravated, and inflammation spreads over the bones surrounding the middle ear [9], [10].

Medical treatment is initial choice to control the active inflammation. Antibiotics are mainly used to eradicate the pathogen in the form of systemic and local deliveries (otic solution). Even if the antibiotic prescription improves the inflammation and secretion of TM, the inflammation may recur as long as structural problems exist in the TM and middle ear. Therefore, a surgical procedure is necessary to fundamentally eliminate the inflammation of the middle ear space and surrounding bone [11], [12]. In some cases, the inflammation in the middle ear cavity is removed during surgical procedure and the perforation is repaired by a graft material. Conductive hearing loss is caused by the inflammatory interruption of sound transmission in the middle ear structure, such as TM and ossicles. The hearing loss is improved by ossiculoplasty, restoration of consecutive morphological structures. The scope and method of detailed surgery depend on the hearing capacity of patients, the condition of the inflammation, and the clinical decision of the otologic surgeon. To evaluate the hearing improvement by surgery, pure-tone audiometry is routinely compared between pre-operatively and post-operatively. Due to the perilous structures, such as the facial nerve, cochlea, brain, and large blood vessels, the surgical operation of COM requires precise and careful handling using a surgical microscope [11]–[14]. The surgical procedure should be performed carefully to avoid the iatrogenic facial nerve injury due to the bony dehiscence covering facial nerve by inflammatory reaction [13]. Although the conventional surgical microscope offers only surface information, the operating procedure depends heavily on the experience and skills of the surgeon due to the lack of sub-surface information of the target region. Over the last century before the invention of the

Manuscript received August 6, 2020; revised September 4, 2020; accepted September 4, 2020. Date of publication September 9, 2020; date of current version October 2, 2020. This work was supported by the Bio & Medical Technology Development Program of the National Research Foundation of Korea (NRF) under Grants MSIP 2017M3A9E2065282 and 2018R1D1A1B07043340. *(Hayoung Kim and Jaeyul Lee contributed equally to this work.) (Corresponding authors: Jeong Hun Jang; Mansik Jeon.)*

Hayoung Kim and Jaeyul Lee are with the School of Electronics and Electrical Engineering, College of IT Engineering, Kyungpook National University, Daegu 41566, South Korea (e-mail: hayoung1101@knu.ac.kr; jaeyul@knu.ac.kr).

Mansik Jeon and Jeehyun Kim are with the School of Electronics and Electrical Engineering, College of IT Engineering, Kyungpook National University, Daegu 41566, South Korea, and also with the School of Electronics Engineering, College of IT Engineering, Kyungpook National University, Daegu 41566, South Korea (e-mail: msjeon@knu.ac.kr; jeehk@knu.ac.kr).

Ruchire Eranga Wijesinghe is with the Department of Biomedical Engineering, College of Engineering, Kyungil University, Gyeongsangbuk-do 38428, South Korea, and also with the Department of Autonomous Robot Engineering, College of Smart Engineering, Kyungil University, Gyeongsangbuk-do 38428, South Korea (e-mail: eranga@kiu.kr).

Jeong Hun Jang is with the Department of Otolaryngology, School of Medicine, Ajou University, Gyeunggi-do 16499, South Korea (e-mail: jhj@ajou.ac.kr).

Color versions of one or more of the figures in this article are available online at https://ieeexplore.ieee.org.

Digital Object Identifier 10.1109/JSTQE.2020.3022927

first otorhinolaryngologic surgical microscope, visualization of anatomical sub-surface has been challenging. [15], [16].

During the last decade, optical coherence tomography (OCT) has been well-utilized intra-operatively for high-resolution sub-surface visualization to improve the proportion of successful operation in otolaryngology and ophthalmology [17]–[20]. Besides its intra-operative applications, OCT techniques over the last two decades have been promisingly recognized for ophthalmology [21]–[23], dentistry [24]–[27], dermatology [28]–[31], and otorhinolaryngology [32], [33]. The high-resolution of OCT (1–15 μm) has vital merits in otology over other medical imaging methods, such as its ability to image a thin sub-surface, low contrast TM, and complicated middle ear structures compared to that of the computed tomography (CT) (50 μm), micro-magnetic resonance imaging (μMRI) (10–100 μm), and positron emission tomography (PET) (1–2 mm) [34], [35]. The unique features of OCT (non-destructive, real-time, and three-dimensional imaging) have a major impact on the surgical maneuver and its recent integration with the microscope [20], [36]–[41]. Several research groups have been able to integrate OCT with surgical microscopes for ophthalmological and otorhinolaryngological applications to aid the visualization of corneal epithelial defects, corneal endothelium, and simulation of surgical maneuvers, such as removal of delusional eyeballs, and corneal penetration [38]–[41]. In otorhinolaryngology, handheld-OCT scanner was developed for TM imaging, which was utilized to intra-operatively differentiate cholesteatoma from inflamed mucosa [42], [43]. However, the above-mentioned methods have surgical constraints due to the short working distance, this therefore causes difficulty in obtaining sufficient space for surgical maneuvers.

In this study, we developed an intra-surgical OCT system to provide effective guidance for surgery on a lesion of the middle ear of three COM patients. The surgical microscope was customized to extend the working distance of the spectral-domain OCT (SD-OCT) system. The intra-surgical OCT system was capable of visualizing sub-surface morphological structures with exceptional resolution. The augmented reality-based OCT image was integrated into the surgical microscope. Depth information of the lesion site was captured and augmented to the ocular eyepiece of the intra-surgical system. Prior to the surgery of OM, the shape of the external auditory meatus and TM was early diagnosed by the otoscopic view and the temporal bone structures were simultaneously investigated by CT scans. The state of the temporal bone and ears was simultaneously observed by CT scans. The acquired cross-sectional images of mastoid bone sites surrounding the TM were visualized through stereoscopic images with the eyepiece view. Depth profiles generated by OCT-based amplitude-scans were also acquired to quantitatively examine the depth information. Furthermore, post-operative audiometric pure-tone diagnostics were performed before and after three months of the surgery to clinically confirm the hearing improvement of each patient. Thus, the results of the study confirmed the feasibility of the developed intra-surgical OCT system followed by post-operative audiogram-based diagnostics, which improves the quality of patient care in otology.

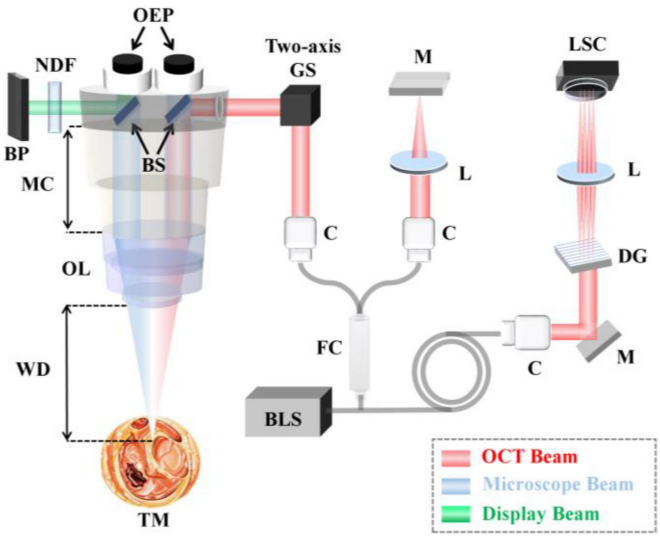

Fig. 1. Schematic of the intra-surgical OCT system. BLS: broadband light source; BP: beam projector; BS: beam splitter; C: collimator; DG: diffracting grating; FC: fiber coupler; L: lens; LSC: line scan camera; M: mirror; MC: magnification changer; NDF: neutral density filter; OEP: ocular eye-piece; OL: objective lens; TM: tympanic membrane; Two-axis GS: two-axis galvano-scanner; WD: working distance.

II. Materials and Methods

A. Surgical Procedure of Patients With Chronic Otitis Media

All the surgical procedures performed in this study were approved under the guidelines and Declaration of Helsinki. The study was approved by the Institutional Review Board of Ajou University Hospital (approval no: AJIRB–DEV–OBS–16–531). Following general anesthesia, the involved three patients with COM were injected with 1:100,000 (v/v) lidocaine and epinephrine to induce local anesthesia. In the external auditory canal, Lempert I, II, and III incisions were made and the Korner flap was elevated. The retroauricular skin was incised and a periosteal flap was elevated using a micro-dissector to expose the external auditory canal, TM, and mastoid cortical bone. With the elevation of the tympanomeatal flap, we removed inflamed tissues in the middle ear cavity. The burr drilling/cutting technique was used to remove the mastoid cortical bone and the exposed antrum. After assessing the mastoid mucosal status, inflammatory tissue was removed using a micro-dissector. Using either autologous bone or an ossicular replacement prosthesis, we performed ossiculoplasty if ossicular discontinuity was evident. The underlying technique was used to insert the temporalis muscle fascia prepared for transplantation into the tympanum. We used our system to evaluate the continuity of the remnant TM, the ossicles, and appropriate graft positioning.

B. Configuration of the Intra-Surgical Optical Coherence Tomography (OCT) System

Fig. 1 shows a schematic diagram of the customized intra-surgical OCT system with augmented reality, which is associated with laboratory customized SD-OCT system. The center wavelength of the employed broadband laser was 846 nm with

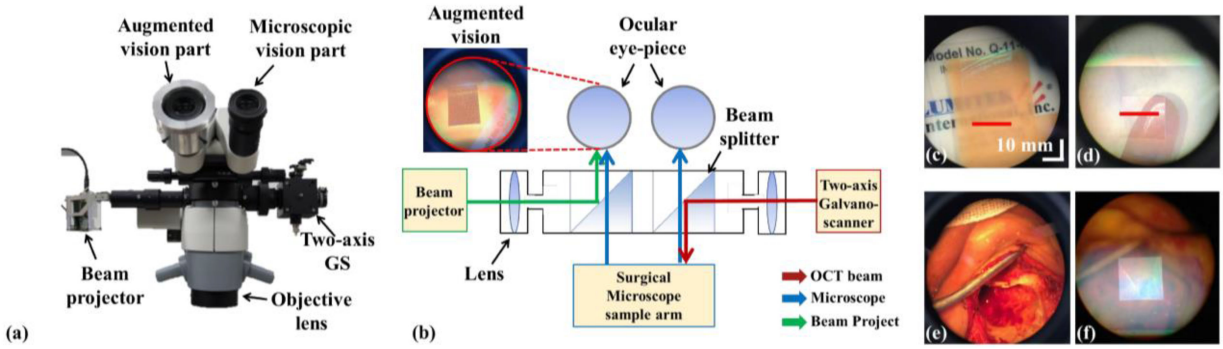

Fig. 2. (a) Surgical head portion of the system; (b) Augmented image acquisition process; (c) Augmented OCT image of infrared detection card on the eyepiece; (d) Augmented OCT image of the fingertip on the eyepiece; (e) Intra-operative image on the eyepiece without augmented OCT image; (f) Intra-operative image on the eyepiece with augmented OCT image.

a bandwidth of 57 nm (SLD–35–HP system; Superlum Ltd.). In air, the OCT system has a lateral resolution of 30 μm and an axial resolution of 8 μm. The sensitivity of the system was 102 dB near-zero delay at an exposure time of 14.1 μs. The two-dimensional images (consist of 500 A-scans) and three-dimensional images (consist of 500 B-scans) were obtained at a field-of-view of $10 \times 10 \times 5$ mm. The OCT working distance was extended to 280 mm, which was mainly adjusted using a magnification changer (MC) (Huvitz Co., Ltd South Korea) that provided sufficient space for surgical handling. The entire magnification device consists of an objective lens (focal length: 225 mm), a tube lens (focal length: 160 mm), and zoom lenses (numerical apertures: 0.015). To confirm the capability of the developed system with extended working distance, the technical aspects are compared with [37], [44].

The interferometer consists of a broadband light source (BLS), sample arm, reference arm, and a spectrometer built with a 2048-pixel line scan camera (LSC) (spl2048-140 km, Basler, Germany). The laser beam was split with a ratio of 50:50 through the fiber coupler (FC) and directed to the reference and sample arms. The beam reflected from the sample arm enters the LSC, thereby causing interference with the beam reflected from the reference arm. An interfering beam from the camera is reconstructed through the computer, which then sends back the completed OCT image to the beam projector (BP).

Fig. 2 shows an illustration of the modified surgical head portion along with the beam propagation and visualization of the OCT image in augmented reality. The augmented-reality microscope consists of an ocular eye-piece (OEP), commercial MC, multiple optical magnification lens configurations, augmented-reality display, and an adjustable microscope head (0° or 30°). The placement of the BP, composition of OEP, and galvano-scanner (GS) are shown in Fig. 2(a). The augmented image acquisition process of the augmented-reality microscope is depicted in Fig. 2(b). Besides the OCT beam path, the visible light reflected by the sample under the augmented-reality microscope is magnified through the objective lens (OL) and MC to enter the OEP as displayed by the blue-colored beam. The OCT image output of the BP (illustrated by the green-colored beam) passes through a neutral density filter (NDF) and is reflected to the augmented vision part of the OEP. The reflected OCT image is overlapped on the existing microscope image. The scanning beam on the infrared detection card is shown in Fig. 2(c), while the augmented reality image of in vivo human finger is shown in Fig. 2(d). The presence of augmented OCT images during surgery is compared in Fig. 2(e) and 2(f). A user-friendly foot pedal was adapted to enable the movements of scanning head position to simply obtain volumetric scans. The customized intra-surgical OCT system was used for the parallel visualization of the surgery along with a surgical microscope to produce a precise real-time cross-sectional evaluation and to confirm the surgical region. Moreover, the key feature of the developed intra-surgical OCT system is the capability of visualizing the whole surgical procedure containing a residue of mastoid inflammation and TM grafting. Additionally, the intra-surgical OCT system was used to visualize residual mastoid air cells. The switching feature (on and off function of the OCT image) was used to obtain a switched visualization between the surgical microscope and the OCT providing a convenient surgical platform for the surgeon. During mastoidectomy and elimination of inflamed tissue, the cross-sections of the intra-surgical OCT visualization was overlapped with the surgical microscopic view, which was useful for the inspection of the surface as well as the sub-surface status of the tissue. The output power of the light source was measured as 4.6 mW. Since only the microscope beam and display beam propagate through the ocular eyepieces, while the infrared OCT beam reflects at the beam splitter with infrared light reflective coating, the use of OEP was not concerned for the exposure of near-infrared light, which was granted according to the ANSI laser safety class.

C. *Clinical Judgment of the Operational Prognosis*

Apart from the method of intra-operative imaging, three additional medical methods, such as otoscopic microscopy, CT, and the pure-tone audiometry were utilized to verify the extent of inflammation, treatments (including surgical procedure), and the prognosis of the operation. A lesion of external auditory meatus and TM were assessed using an otoscopic microscope to confirm the necessity of a surgical procedure. The TM status was compared between pre-operatively and post-operatively for the diagnosis of the exact middle ear condition and evaluating the

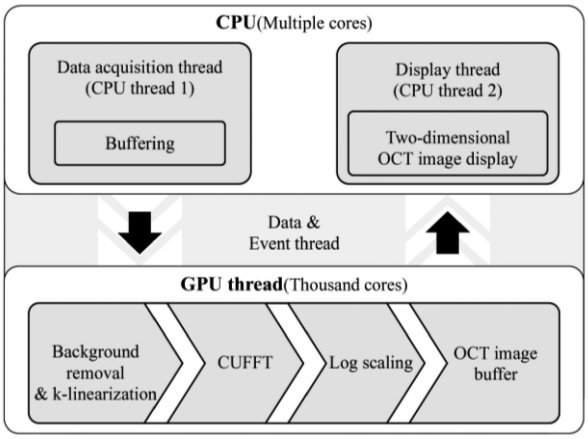

Fig. 3. Flowchart describing the algorithm of intra-surgical OCT image acquisition.

surgical outcome. The destructive status of middle ear structure including ossicles and mastoid cavity using the temporal bone was confirmed through CT scans. Pure-tone audiometry was conducted to identify the hearing status of patients with COM prior to the surgery. The pure-tone was electrically generated to control the intensity of sound at each frequency and to measure the level of hearing. Multiple audible frequency levels starting from 125 Hz, 250 Hz, 500 Hz, 1000 Hz, 2000 Hz, and 8000 Hz were used through the audiometer and the minimum audible threshold frequency of each patient was recorded.

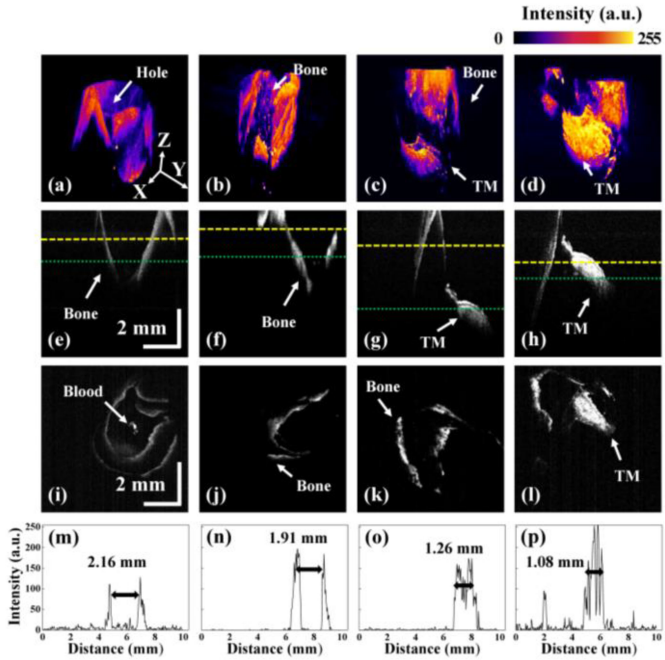

Fig. 4. Assessment of the mastoid bone and tympanic membrane of COM lesion. (a)–(d) volumetric OCT images of human TM and its surrounding bony structures; (e) and (f) cross-sectional OCT images of bony structure; (g) and (h) cross-sectional OCT images of TM; (i)-(l) representative en-face OCT images acquired from the corresponding depth range indicated with yellow dashed line; (m)–(p) representative lateral direction A-scan profiles acquired from the indicated green color-dotted lines.

D. GPU-Based Image Construction Algorithm for OCT Augmented Display

Fig. 3 illustrates a graphical overview of the laboratory customized image acquisition and processing algorithm of the intra-surgical OCT system. The experiment was performed for the patients in real-time. Thus, to overcome motion artifacts during the surgical procedure, multiple cores of the central processing unit (CPU) and the thousand cores of graphics processing unit (GPU) threads were well-utilized for the parallel processing of the data and event threads to enhance the image acquisition processing speed in the actual surgical environment. The acquired OCT signals through a frame grabber were subjected to the repeated buffering in the data acquisition thread of the CPU and then sent to the GPU thread. The removal of noise and background signals, wave-number linearization, CUDA fast Fourier transform (CUFFT), log scaling, and the OCT image buffer were conducted accordingly on the CUDA kernels [45].

Finally in the CPU threads, a two-dimensional OCT (2D-OCT) image is displayed in real-time with enhanced OCT frame rate.

III. Results and Discussion

Volumetric, cross-sectional, and en-face OCT images of human mastoid bone and the TM during COM surgery were visualized with A-scan intensity profiles as shown in Fig. 4. Through the acquisition of the entire OCT data of the scanned region, three-dimensional images were formed as shown in Fig. 4(a)–4(d). The position and shape of the mastoid bone and TM were identified. The cross-sectional OCT images as shown in Fig. 4(e)–4(h) supported the depth information and TM shape through augmented reality using the intra-surgical OCT system, while providing a precise visualization of the depth and thickness of the desired region of interest in real-time during surgery. The intensity difference indicates the morphological inner structures and depth-directional structural information. The exact locations of en-face image extraction are indicated using yellow-dashed line in Fig. 4(e)–4(h). The en-face images (Fig. 4(i)–4(l)) visualized the hole surrounded by the mastoid bone, blood, and TM region. The green dotted line of each figure indicates the exact lateral region, which was used to extract the intensity profile (Fig. 4(m)–4(p)). The depth profile is beneficial to obtain quantitative measurements of the distance of dipped area and thickness of the TM region. The morphological structures of TM and mastoid bone with surrounding locations were more effectively assessed using volumetric, cross-sectional, and en-face images.

The 2D and en-face OCT representations emphasize the successful removal of infected tissues, where inflammation is no longer visualizable. Since grayscale OCT images sufficiently reveal the soft bony structures with the removal of inflammation, lateral direction intensity quantifications were further assessed to verify the thickness information numerically as shown in amplitude scans of Fig. 4. Since the visualization of structural

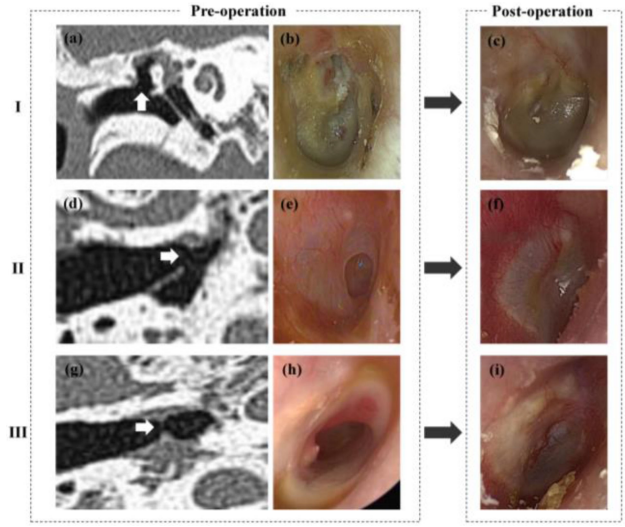

Fig. 5. (a), (d), and (g) Pre-operative CT coronal view of the temporal bone; (b), (e) and (h) Pre-operative microscopic view of TM; (c), (f), and (i) Post-operative otoscopic view of the TM acquired after three months; The white arrows indicate bony erosion in the attic area, respectively.

information is necessary to remove inflammation more precisely, the skills of the surgeon can be further enhanced by using the augmented reality-based intra-surgical OCT system.

Fig. 5 describes the CT scans of temporal bone and otoscopic view of TM perforation, which were acquired pre-operatively and post-operatively in the three patients. The coronal view of CT scan indicates bony erosion of attic area in Fig. 5(a), 5(d) and 5(g). The bony erosions (white arrows) are important clinical findings for diagnosis of and determination of surgery. The pre-operative otoscopic views reveal the perforation and inflammation of TM, where inflammatory debris and discharge cover the TM as shown in Fig. 5(b), 5(e), and 5(h). The large perforations of TM were also distinctly confirmed by the otoscopic views of Fig. 5(e) and 5(h). The reconstructions of TM were identified at post-operative three months with the removal of the inflammation as shown in Fig. 5(c), 5(f), and 5(i).

The pre-operative and post-operative pure-tone audiograms were measured to identify the hearing gain as shown in Fig. 6. During bone conduction (BC), the sound signal bypasses the outer or middle ear, which is transmitted directly to the inner ear. Bone conduction threshold shows the hearing status of neural component. The degree of air conduction (AC) and bone conduction threshold difference, which is represented to air-bone gap (ABG) is the definitive clue for determining the abnormality of the external or middle ear [46]. The mean ABG is expected to be 0 dB for normal hearing and sensorineural hearing loss. Normally, it is regarded as an abnormality in external ear or middle ear when the ABG exceeds 10 dB, while it will be categorized as conductive hearing loss when the value exceeds 20 dB. The mean ABG values of the 500 Hz, 1 kHz, 2 kHz, and 4 kHz were measured as 30.0 dB, 15.0 dB, 41.3 dB by the patient I, II, and III, respectively as shown in Fig. 6(a), 6(c), and 6(e). At post-operative three months, the mean ABG

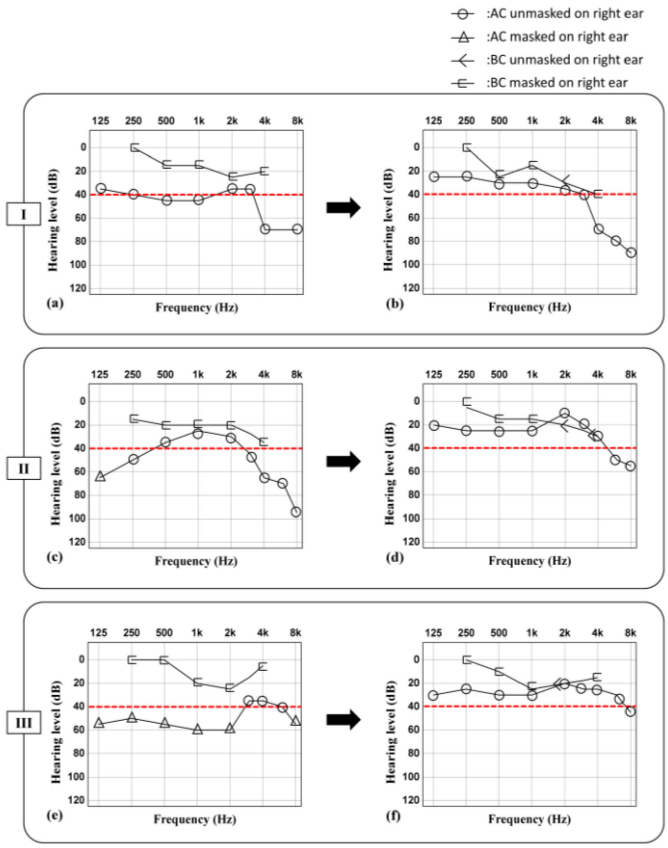

Fig. 6. Pure-tone audiometric evaluation of the pre-operation and post-operation with three COM patients; (a), (c), and (e) Pure-tone audiograms at pre-operation with comparing AC and BC hearing test; (b), (d), and (f) Pure-tone audiograms at post-operation acquired after three months with comparing AC and BC hearing test; The red-dashed lines indicate the level of serviceable hearing.

values were enhanced to 13.8 dB, 7.5 dB, and 8.8 dB with an increased percentage of 54%, 50%, and 79% of each patient I, II, and III as shown in Fig. 6(b), 6(d), and 6(f). The average improvement ratio of all patients was evaluated by 61%. Given that the difference was significantly reduced post-operatively, and it can be confirmed that the surgery was well-performed base on ABG reduction. The red-dashed line drawn according to the 40 dB value indicates the level of serviceable hearing, which is the minimum hearing requirement for smooth conversation as shown in Fig. 6. Most hearing levels recorded from 125 Hz to 4 kHz in the pre-operative pure-tone audiograms exceeded the serviceable hearing level. Both air and bone conduction hearing thresholds are marked within 40 dB and confirm that the problem has been resolved through the surgical procedure with the support of the intra-surgical OCT system.

According to these results of pure-tone audiogram, surgical procedure can be deemed to be sufficiently well accomplished by the real-time intraoperative imaging of COM using the intra-surgical OCT system. The real-time cross-sectional OCT images exhibit the depth-directional information for better guidance of the targeted region during the surgery. CT and otoscopic examinations were certainly necessary techniques for

pre-operative diagnosis. Although the surgical microscope was combined with OCT to effectively guide the surgical procedures for enhancing the successful completeness of the COM surgery, it was initially difficult to deduce that the surgical procedure was completed successfully compared to conventional operating methods. Thus, the surgical outcome was clinically assessed using the pre-operative and post-operative pure-tone audiometry.

IV. Conclusion

The developed intra-surgical OCT system has been utilized to support the COM operation with enhanced working distance of 280 mm. The augmented reality stably provides real-time cross-sectional OCT images that simultaneously overlaps with the surgical microscope image on the eyepiece. The key insight of the current study is the enhanced clinical efficacy through the obtained real-time intra-operative OCT assessments followed by post clinical evaluations using multiple existing clinical techniques. The hearing restoration by the reconstruction of TM and ossicular structure using TM graft and ossicular replacement was assessed by the comparison of the pre-operative and post-operative pure-tone audiograms. The measured ABG values of the audiogram indicated the hearing improvement, where the overall hearing threshold has been satisfied within 40 dB HL. The audiogram results obtained after the surgery revealed that the mean hearing threshold of all patients was enhanced with a 61% hearing capability compared to pre-operative threshold, which confirms the success of the surgical procedure. The overall result of the proposed scheme clearly emphasizes the potential merits of the developed augmented-reality intra-operative OCT system as a valuable aid to surgeons and conventional surgical procedures, which will in turn enhance the accuracy of the procedure followed by the verification obtained through pure-tone audiogram evaluations. Further research studies are therefore can be encouraged to enhance the surgical outcomes with the post-operative audiogram-based diagnostics to expand the regular utilization of the system in the operating theatre.

References

[1] F. Zhao, T. Koike, J. Wang, H. Sienz, and R. Meredith, "Finite element analysis of the middle ear transfer functions and related pathologies," *Med. Eng. Phys.*, vol. 31, pp. 907–916, 2009.

[2] Y. Onchi, "Mechanism of the middle ear," *J. Acoustical Soc. America*, vol. 33, pp. 794–805, 1961.

[3] B. Ars, "Organogenesis of the middle ear structures," *J. Laryngol. Otol.*, vol. 103, pp. 16–21, 1989.

[4] I. Brook and S. M. Finegold, "Bacteriology of chronic otitis media," *Jama*, vol. 241, pp. 487–488, 1979.

[5] W. L. Meyerhoff, C. S. Kim, and M. M. Paparella, "Pathology of chronic otitis media," *Ann. Otol., Rhinol. Laryngol.*, vol. 87, pp. 749–760, 1978.

[6] Y. S. Liu, D. J. Lim, R. Lang, and H. G. Birck, "Microorganisms in chronic otitis media with effusion," *Ann. Otol., Rhinol. Laryngol.*, vol. 85, pp. 245–249, 1976.

[7] R. Sugita, S. Kawamura, G. Ichikawa, S. Goto, and Y. Fujimaki, "Studies on anaerobic bacteria in chronic otitis media," *laryngoscope*, vol. 91, pp. 816–821, 1981.

[8] L. Hall-Stoodley *et al.*, "Direct detection of bacterial biofilms on the middle-ear mucosa of children with chronic otitis media," *Jama*, vol. 296, pp. 202–211, 2006.

[9] R. A. Chole and H. H. Sudhoff, "Chronic otitis media, mastoiditis, and petrositis," *Cummings Otolaryngol. Head Neck Surgery*, vol. 3, pp. 1963–1978, 1998.

[10] G. M. English, J. L. Northern, and T. J. Fria, "Chronic otitis media as a cause of sensorineural hearing loss," *Archives Otolaryngol.*, vol. 98, pp. 18–22, 1973.

[11] U. Fisch, J. S. May, and T. Linder, in *Tympanoplasty, Mastoidectomy, and Stapes Surgery*, 2nd ed.n. London, U.K.: The royal college of surgeons of England, 2010.

[12] S. Albu, G. Babighian, and F. Trabalzini, "Prognostic factors in tympanoplasty," *Amer. J. Otol.*, vol. 19, pp. 136–140, 1998.

[13] S. H. Selesnick and A. G. Lynn-Macrae, "The incidence of facial nerve dehiscence at surgery for cholesteatoma," *Otol. Neurotol.*, vol. 22, pp. 129–132, 2001.

[14] M. T. Chuang, I. C. Chiang, G. C. Liu, and W. C. Lin, "Multidetector row CT demonstration of inner and middle ear structures," *Clin. Anatomy: Official J. Amer. Assoc. Clin. Anatomists Brit. Assoc. Clin. Anatomists*, vol. 19, pp. 337–344, 2006.

[15] E. Vartiainen and M. Kansanen, "Tympanomastoidectomy for chronic otitis media without cholesteatoma," *Otolaryngol.—Head Neck Surgery*, vol. 106, pp. 230–234, 1992.

[16] B. J. Gantz, E. P. Wilkinson, and M. R. Hansen, "Canal wall reconstruction tympanomastoidectomy with mastoid obliteration," *laryngoscope*, vol. 115, pp. 1734–1740, 2005.

[17] S. A. Boppart *et al.*, "Intraoperative assessment of microsurgery with three-dimensional optical coherence tomography," *Radiology*, vol. 208, pp. 81–86, 1998.

[18] J. G. Fujimoto, C. Pitris, S. A. Boppart, and M. E. Brezinski, "Optical coherence tomography: An emerging technology for biomedical imaging and optical biopsy," *Neoplasia*, vol. 2, 2000.

[19] A. M. Zysk, F. T. Nguyen, A. L. Oldenburg, D. L. Marks, and S. A. Boppart, "Optical coherence tomography: A review of clinical development from bench to bedside," *J. Biomed. Opt.*, vol. 12, 2007, Art. no. 051403.

[20] J. Lee *et al.*, "Clinical utility of intraoperative tympanomastoidectomy assessment using a surgical microscope integrated with an optical coherence tomography," *Scientific Rep.*, vol. 8, pp. 1–8, 2018.

[21] J. G. Fujimoto, W. Drexler, J. S. Schuman, and C. K. Hitzenberger, "Optical Coherence Tomography (OCT) in ophthalmology: Introduction," *Opt. Express*, vol. 17, pp. 3978–3979, 2009.

[22] D. Matsunaga, J. Yi, C. A. Puliafito, and A. H. Kashani, "OCT angiography in healthy human subjects," *Ophthalmic Surgery, Lasers Imag. Retina*, vol. 45, pp. 510–515, 2014.

[23] J. Park *et al.*, "Biocompatibility evaluation of bioprinted decellularized collagen sheet implanted in vivo cornea using swept-source optical coherence tomography," *J. Biophoton.*, vol. 12, 2019, Paper e201900098.

[24] J. Lee *et al.*, "Classification of human gingival sulcus using swept-source optical coherence tomography: In vivo imaging," *Infrared Phys. Technol.*, vol. 98, pp. 155–160, 2019.

[25] Y. Shimada*et al.*, "Validation of swept-source optical coherence tomography (SS-OCT) for the diagnosis of occlusal caries," *J. Dentistry*, vol. 38, pp. 655–665, 2010.

[26] J. Lee *et al.*, "Identification of multi-dimensional thread geometry using depth-resolved swept-source optical coherence tomography for assessment of dental implant fabrication," *Opt. Lasers Eng.*, vol. 127, 2020, Art. no. 105951.

[27] S. Lee *et al.*, "Non-ionized, high-resolution measurement of internal and marginal discrepancies of dental prosthesis using optical coherence tomography," *IEEE Access*, vol. 7, pp. 6209–6218, 2018.

[28] M. C. Pierce, J. Strasswimmer, B. H. Park, B. Cense, and J. F. De Boer, "Advances in optical coherence tomography imaging for dermatology," *J. Investigative Dermatol.*, vol. 123, pp. 458–463, 2004.

[29] T. Gambichler, V. Jaedicke, and S. Terras, "Optical coherence tomography in dermatology: Technical and clinical aspects," *Archives dermatological Res.*, vol. 303, pp. 457–473, 2011.

[30] M. Mogensen, L. Thrane, T. M. Jørgensen, P. E. Andersen, and G. B. Jemec, "OCT imaging of skin cancer and other dermatological diseases," *J. Biophoton.*, vol. 2, pp. 442–451, 2009.

[31] R. E. Wijesinghe, K. Park, D.-H. Kim, M. Jeon, and J. Kim, "In vivo imaging of melanoma-implanted magnetic nanoparticles using contrast-enhanced magneto-motive optical Doppler tomography," *J. Biomed. Opt.*, vol. 21, 2016, Art. no. 064001.

[32] J. Lee *et al.*, "Decalcification using ethylenediaminetetraacetic acid for clear microstructure imaging of cochlea through optical coherence tomography," *J. Biomed. Opt.*, vol. 21, 2016, Art. no. 081204.

[33] R. Heermann, C. Hauger, P. Issing, and T. Lenarz, "Application of optical coherence tomography (OCT) in middle ear surgery," *Laryngo-Rhino-Otologie*, vol. 81, pp. 400–405, 2002.

[34] H. E. I. Tan *et al.*, "Optical coherence tomography of the tympanic membrane and middle ear: A review," *Otolaryngology–Head Neck Surgery*, vol. 159, pp. 424–438, 2018.
[35] N.-H. Cho, U.-S. Jung, H.-I. Kwon, H.-S. Jeong, and J.-H. Kim, "Development of SD-OCT for imaging the in vivo human tympanic membrane," *J. Opt. Soc. Korea*, vol. 15, pp. 74–77, 2011.
[36] T. Hellmuth, M. Kaschke, J. C. Moore, and G. Unold, in *OCT-Assisted Surgical Microscope With Multi-Coordinate Manipulator*. Google Patents, 1998.
[37] E. Lankenau *et al.*, "Combining optical coherence tomography (OCT) with an operating microscope," in *Advances in Medical Engineering*. Berlin, Germany: Springer, 2007, pp. 343–348.
[38] J. P. Ehlers*et al.*, "Integrative advances for OCT-guided ophthalmic surgery and intraoperative OCT: Microscope integration, surgical instrumentation, and heads-up display surgeon feedback," *PloS One*, vol. 9, 2014.
[39] N. H. Cho, J. H. Jang, W. Jung, and J. Kim, "In vivo imaging of middle-ear and inner-ear microstructures of a mouse guided by SD-OCT combined with a surgical microscope," *Opt. Express*, vol. 22, pp. 8985–8995, 2014.
[40] P. Reimer, C. Hauger, A. Abele, and M. Seesselberg, in *Ophthalmic Surgical Microscope Having an OCT-system*. Google Patents, 2010.
[41] Y. K. Tao, S. K. Srivastava, and J. P. Ehlers, "Microscope-integrated intraoperative OCT with electrically tunable focus and heads-up display for imaging of ophthalmic surgical maneuvers," *Biomed. Opt. Express*, vol. 5, pp. 1877–1885, 2014.
[42] W. Jung*et al.*, "Handheld optical coherence tomography scanner for primary care diagnostics," *IEEE Transa. on Biomed. Eng.*, vol. 58, no. 3, pp. 741–744, Mar. 2011.
[43] H. R. Djalilian, J. Ridgway, A. S. M. Tam, Z. Chen, and B. J. Wong, "Imaging the human tympanic membrane using optical coherence tomography in vivo," *Otology Neurotology: Official Publication Amer. Otological Soc., Amer. Neurotol. Soc. Eur. Acad. Otol. Neurotol.*, vol. 29, 2008, Art. no. 1091.
[44] J. P. Ehlers*et al.*, "Integrative advances for OCT-guided ophthalmic surgery and intraoperative OCT: Microscope integration, surgical instrumentation, and heads-up display surgeon feedback," *PloS One*, vol. 9, pp. e105224, 2014.
[45] S. Van der Jeught, A. Bradu, and A. G. Podoleanu, "Real-time resampling in Fourier domain optical coherence tomography using a graphics processing unit," *J. Biomed. Opt.*, vol. 15, 2010, Art. no. 030511.
[46] H.-Y. Lin *et al.*, "Assessment of hearing loss by pure-tone audiometry in patients with mucopolysaccharidoses," *Mol. Genetics Metabolism*, vol. 111, pp. 533–538, 2014.

Hayoung Kim received the B.E. degree in electronics engineering in 2018 from Kyungpook National University, Daegu, South Korea, where he is currently working toward the M.S. degree with the Department of Electronics Engineering. His research interests are the development of biomedical imaging systems, including optical coherence tomography, photoacoustic tomography, and their clinical applications.

Jaeyul Lee is currently working toward the Ph.D. degree with the School of Electronics Engineering, Kyungpook National University, Daegu, South Korea. His research interests are in the development of high-resolution novel imaging techniques and optical imaging techniques including photoacoustic microscopy, optical coherence tomography, optical coherence angiography, handheld instruments, and their biomedical applications.

Ruchire Eranga Wijesinghe received the B.Sc. and Ph.D. degrees in electronics engineering from Kyungpook National University, Daegu, South Korea, in 2012 and 2018, respectively. He is currently an Assistant Professor with the Department of Biomedical Engineering, Kyungil University, Gyeongsan, South Korea. His research interests are in the development of high-resolution novel biological and biomedical imaging techniques including optical coherence tomography and microscopy for clinical utility.

Jeong Hun Jang received the M.D. and Ph.D. degrees from Seoul National University, Seoul, South Korea, in 2001 and 2013, respectively. He is currently an Associate Professor with the Department of Otorhinolaryngology, Ajou University College of Medicine, Suwon, South Korea. His research interests focus on clinical and basic research for cochlear implant and clinical application of optical coherence tomography in otology.

Mansik Jeon (Member, IEEE) received the Ph.D. degree in electronics engineering from Kyungpook National University, Daegu, South Korea, in 2011. He is currently an Associate Professor with the School of Electronics Engineering, Kyungpook National University. His research interests are in the development of nonionizing and noninvasive novel biomedical imaging techniques, including photoacoustic tomography, photoacoustic microscopy, optical coherence tomography, ultrasonic imaging, handheld scanner, and their clinical applications.

Jeehyun Kim (Member, IEEE) received the Ph.D. degree in biomedical engineering from the University of Texas at Austin, Austin, TX, USA, in 2004. He has worked as a Postdoctoral Researcher with the University of California, Irvine, at Beckman Laser institute. He is currently a Professor with Kyungpook National University, Daegu, South Korea. His research interests include biomedical imaging and sensing, neuroscience studies using multiphoton microscopy, photo-acoustic imaging and other novel applications of sensors.